PHYSICAL REVIEW D **83,** 123510 (2011)

# Kinetic analysis of thermally relativistic flow with dissipation. II. Relativistic Boltzmann equation versus its kinetic models

Ryosuke Yano,[1,*] Jun Matsumoto,[2] and Kojiro Suzuki[1,†]

[1]*Department of Advanced Energy, University of Tokyo, 5-1-5 Kashiwanoha, Kashiwa, Chiba 277-8561, Japan*
[2]*Department of Aeronautics and Astronautics, University of Tokyo, 7-3-1, Hongo, Bunkyo, Tokyo, 113-8656, Japan*
(Received 22 April 2011; published 7 June 2011)

Thermally relativistic flow with dissipation was analyzed by solving the rarefied supersonic flow of thermally relativistic matter around a triangle prism by Yano and Suzuki [Phys. Rev. D **83**, 023517 (2011)], where the Anderson-Witting (AW) model was used as a solver. In this paper, we solve the same problem, which was analyzed by Yano and Suzuki, using the relativistic Boltzmann equation (RBE). To solve the RBE, the conventional direct simulation Monte Carlo method for the nonrelativistic Boltzmann equation is extended to a new direct simulation Monte Carlo method for the RBE. Additionally, we solve the modified Marle (MM) model proposed by Yano-Suzuki-Kuroda for comparisons. The solution of the thermally relativistic shock layer around the triangle prism obtained using the relativistic Boltzmann equation is considered by focusing on profiles of macroscopic quantities, such as the density, velocity, temperature, heat flux and dynamic pressure along the stagnation streamline (SSL). Differences among profiles of the number density, velocity and temperature along the SSL obtained using the RBE, the AW and MM. models are described in the framework of the relativistic Navier-Stokes-Fourier law. Finally, distribution functions on the SSL obtained using the RBE are compared with those obtained using the AW and MM models. The distribution function inside the shock wave obtained using the RBE does not indicate a bimodal form, which is obtained using the AW and MM models, but a smooth deceleration of thermally relativistic matter inside a shock wave.

DOI: 10.1103/PhysRevD.83.123510 PACS numbers: 98.80.Jk, 25.75.−q, 47.75.+f

## I. INTRODUCTION

Relativistic flow with dissipation is a significant issue in the fields of high-energy physics. In particular, the thermalization (relaxation) of the pre-equilibrium state of the quark gluon, namely, glasma [1], into the equilibrium state has been studied analytically or experimentally using a relativistic heavy ion collider such as the Relativistic Heavy Ion Collider (RHIC) [2] or the Large Hadron Collider (LHC) [3]. The analytical difficulties in such a relaxation process of glasma depends on the intricate system composed of quarks and gluons. Such an intricate system cannot be described by the relativistic Boltzmann equation (RBE) coupled to the Yang-Mills equation [4], because the strongly coupled partons yield the multibody correlations, which cannot be formulated by binary collisions formulated by the RBE. Actually, the kinetic approach to glasma on the basis of the RBE was extended to three body correlations of gluons by Xu and Greiner [5]. On the other hand, analytical studies of the relativistic kinetic theory based on the RBE have been developed by Israel [6] Stewart [7] and Müller-Ruggeri [8] since the proposal of the relativistic equilibrium function by Jüttner [9], whereas the numerical studies of the relativistic fluid with dissipation have been developed by the BAMPS [10] or SHASTA [10]. As an initial approach to elucidating the dynamics of glasma, there exists a hydrodynamic interest in the relativistic fluid with dissipation, such as relativistic shock waves, expansion waves, boundary (shear) layers and vortices. Here, we consider not glasma composed of the quarks and gluons but thermally relativistic matter [11] composed of hard sphere particles, because the discussion of thermally relativistic matter composed of hard sphere particles instead of glasma can be presumably meaningful as an initial approach to studying the relativistic flow of quarks and gluons with dissipation.

In our recent numerical study of the relativistic flow with dissipation [11], the relativistic shock wave, expansion wave, boundary (shear) layer and vortices were analyzed by solving the rarefied supersonic flow of thermally relativistic matter composed of hard sphere particles around a triangle prism. Such a study of the shock layer composed of thermally relativistic matter around a triangle prism is significant for the comprehension of the Mach cone [12], which is considered to be generated by fast partons through hot and dense matter during Au + Au collision in the RHIC. As a solver of thermally relativistic flow with dissipation, one of relativistic Boltzmann-kinetic equations, namely, the Anderson-Witting (AW) model [13], was used. In this paper, we analyze one of the problems, which was discussed using the AW model in previous study [11], using the RBE and modified Marle (MM) model proposed by Yano-Suzuki-Kuroda [14]. We solve the forward a triangle prism to focus on the shock wave and thermal boundary

*yano@daedalus.k.u-tokyo.ac.jp
†kjsuzuki@k.u-tokyo.ac.jp

 

layer. As a solver of the RBE, the conventional direct simulation Monte Carlo (DSMC) method for the nonrelativistic Boltzmann equation [15] was extended to a new DSMC method for the RBE using the majorant frequency scheme [16] in Sec. III, whereas the past work [5,17] used the DSMC method on the basis of the Bird's scheme [15], whose computational time is markedly longer than the majorant frequency scheme. The aim of this study is the comparison of numerical results on thermally relativistic flow with dissipation obtained using the RBE, AW and MM models, because such a comparison is useful for understanding dissipation in the RBE, AW and MM models. Consequently, our numerical results are presumably useful as an initial study of the Mach cone generated by fast partons through hot and dense matter during Au + Au collision in the RHIC.

The profiles of the density, velocity, temperature, heat flux and dynamic pressure, obtained by the Eckart decomposition [18], along the stagnation streamline (SSL) obtained using the RBE are compared with those obtained using the AW and MM models. The profiles of the number density, velocity and temperature along the SSL obtained using the RBE are different from those obtained using the AW and MM models in the shock wave and thermal boundary layer. In particular, the location of the shock wave obtained using the RBE is farther toward the wall than those obtained using the AW and MM models, because of the thickest thermal boundary layer obtained using the RBE, which is derived from the smallest Prandtl number obtained using the RBE. The shock wave obtained using the RBE is thinner than those obtained using the AW and MM models, because of its larger collision frequency than those obtained using the AW and MM models. Heat fluxes along the SSL obtained using the RBE, AW and MM models can be approximated by the relativistic Navier-Stokes-Fourier (RNSF) law except for the strong nonequilibrium regime inside the shock wave, whereas dynamic pressures obtained using the RBE, AW and MM models cannot be approximated by the RNSF law. Finally, the distribution functions on the SSL obtained using the RBE are compared with those obtained using the AW and MM models. The distribution function inside the shock wave obtained using the RBE indicates not a bimodal form, which is obtained using the AW and MM models, but a smooth deceleration of thermally relativistic matter inside the shock wave.

This paper is organized as follows. In Sec. II, we review the RBE, AW and MM models. In Sec. III, the numeric of the RBE using the DSMC method [15] is described. In. Sec. IV, the numerical analysis of the rarefied supersonic flow around a triangle prism is discussed. Finally, concluding remarks are given in Sec. V.

## II. RELATIVISTIC BOLTZMANN EQUATION AND ITS KINETIC MODELS

The relativistic Boltzmann equation is written as [19]

$$p^\alpha \frac{\partial f}{\partial x^\alpha} = Q(f,f) = \int_{\mathcal{R}^3}\int_{\Omega^2}(f'_* f' - f_* f) F \sigma d\Omega \frac{d^3\mathbf{p}_*}{p_{*0}}, \tag{1}$$

where $x^\alpha$ represents the four-dimensional coordinates, $p^\alpha$ is the four momentum, $f$ is the distribution function defined by $f = f(t, x^i, p^i)(i = 1, 2, 3)$, and $F$ is the Lorentz invariant flux. In Eq. (1), terms with a prime indicate conditions after collisions, $\Omega^2$ is the solid angle space and $\mathcal{R}^3$ is the momentum space stretched by $\{\mathcal{R}^3 | (-\infty, -\infty, -\infty) \le (p^1, p^2, p^3) \le (\infty, \infty, \infty)\}$. $x^\alpha$, $p^\alpha$ and $F$ are given by

$$x^\alpha = (ct, x^1, x^2, x^3), \tag{2}$$

$$p^\alpha = m\gamma(v)(c, v^1, v^2, v^3), \tag{3}$$

$$F = \frac{p^0 p^0_*}{c} g_\emptyset = \frac{p^0 p^0_*}{c}\sqrt{(\boldsymbol{v}-\boldsymbol{v}_*)^2 - \frac{1}{c^2}(\boldsymbol{v}\times\boldsymbol{v}_*)^2} \quad \left(\because g_\emptyset = \sqrt{(\boldsymbol{v}-\boldsymbol{v}_*)^2 - \frac{1}{c^2}(\boldsymbol{v}\times\boldsymbol{v}_*)^2}\right)$$
$$= \sqrt{(p^\alpha_* p_\alpha)^2 - m^4 c^4}. \tag{4}$$

In Eq. (3), $\gamma(v)$ is the Lorentz factor, which is defined by $\gamma(v) = 1/\sqrt{1 - v^2/c^2}$. $c$ is the speed of light and $v^i$ $(i = 1, 2, 3)$ is the $i$th component of the particle velocity vector $\boldsymbol{v} = (v^1, v^2, v^3)$. In Eqs. (3) and (4), $m$ is the molecular mass. In Eq. (4), $g_\emptyset$ is Møller's relative velocity. In Eq. (1), $\sigma$ is the differential cross section and $d\Omega$ is the solid angle element. In Eqs. (1) and (4), terms with an asterisk subscript belong to the collision partner.

Rewriting Eq. (1) in Lorentz variant form yields

$$\frac{\partial f}{\partial t} + v^i \frac{\partial f}{\partial x^i} = \int_{\mathcal{R}^3}\int_{\Omega^2}(f'_* f' - f_* f) g_\phi \sigma d\Omega d^3\mathbf{p}_*. \tag{5}$$

In the rest of this section, we describe two kinetic equations, namely, the AW and MM models. The AW model is written as [13]

$$p^\alpha \frac{\partial f}{\partial x^\alpha} = \frac{U_L^\alpha p_\alpha}{c^2 \tau}(f^{(0)} - f), \tag{6}$$

where $f^{(0)}$ is an equilibrium function called the Maxwell-Jüttner function defined by

$$f^{(0)}(n, \theta_E, u^i) = \frac{n}{4\pi m^2 c k \theta_E K_2(\zeta_E)} e^{-((U^\alpha p_\alpha)/(k\theta_E))}, \tag{7}$$

where $i = 1, 2, 3$, $n$ is the number density, $u^i$ is the $i$th component of the flow velocity vector $\boldsymbol{u} = (u^1, u^2, u^3)$, $\zeta_E$ is given by $\zeta_E = \frac{mc^2}{k\theta_E}$, $k$ is the Boltzmann constant, $\theta_E$ is the temperature used in the equilibrium function $f^{(0)}$ and $U^\alpha$ is the four velocity of flow defined by (A5). $K_n$ is the $n$th order modified Bessel function of the second kind and $U_L^\alpha$ is the four velocity defined by Landau-Lifshitz [20] and written as

$$U_L^\alpha = U^\alpha + \frac{q^\alpha}{ne + p}, \tag{8}$$

where $q^\alpha$ is the heat flux, $e$ is the energy density and $p$ is the static pressure.

The relaxation rate $\tau$ in Eqs. (6) is given for a hard sphere particle by [19]

$$\tau = \frac{1}{n\sigma_T \langle g_\emptyset \rangle} \simeq \frac{1}{n\sigma_T v_s}, \tag{9}$$

where $\sigma_T = \pi d^2$ ($d$: the diameter of a particle) is the total collision cross section, $\langle g_\emptyset \rangle$ is the average of the Møller's relative velocity. We use the approximation $\langle g_\emptyset \rangle \simeq v_s$ [19], where $v_s$ is the relativistic speed of sound defined by

$$v_s = \sqrt{\frac{\zeta^2 + 5G\zeta - G^2\zeta^2}{G(\zeta^2 + 5G\zeta - G^2\zeta^2 - 1)}} \frac{k\theta}{m}, \tag{10}$$

where $\zeta = \frac{mc^2}{k\theta}$, at which $\theta$ is the temperature of matter, and $G \equiv K_3(\zeta)/K_2(\zeta)$.

For the conservation law for $N^\alpha$ and $T^{\alpha\beta}$ in Eqs. (A1) and (A2), the following constraints must be satisfied:

$$c\int_{\mathcal{R}^3} p^\alpha U_{L\alpha} f \frac{d^3\mathbf{p}}{p^0} = N^\alpha U_{L\alpha} = c\int_{\mathcal{R}^3} p^\alpha U_{L\alpha} f^{(0)} \frac{d^3\mathbf{p}}{p^0} = N_E^\alpha U_{L\alpha}, \tag{11}$$

$$c\int_{\mathcal{R}^3} p^\alpha p^\beta U_{L\alpha} f \frac{d^3\mathbf{p}}{p^0} = T^{\alpha\beta} U_{L\alpha} = c\int_{\mathcal{R}^3} p^\alpha p^\beta U_{L\alpha} f^{(0)} \frac{d^3\mathbf{p}}{p^0} = T_E^{\alpha\beta} U_{L\alpha}, \tag{12}$$

where the subscript $E$ indicates the quantities derived from the equilibrium distribution function $f^{(0)}$. These constraints are considered to be satisfied by the orthogonality of $U_L^\alpha$ to nonequilibrium terms in either $N^\alpha$ or $T^{\alpha\beta}$ [19]. Multiplying Eq. (12) by $U_{L\beta}/(nc^2)$, we obtain [19,20]

$$e_E = e. \tag{13}$$

This relation yields the following equality from the relation $e = mc^2(G(\zeta) - \frac{1}{\zeta})$

$$\theta_E = \theta. \tag{14}$$

In the AW model, $\theta_E$ is the temperature used in the equilibrium function $f^{(0)}$, which is equal to $\theta$, the temperature of matter.

The Marle model [21] is obtained by replacing $\frac{U_L^\alpha p_\alpha}{c^2}$ in Eq. (6) with $m$.

The Marle model is written as [21]

$$p^\alpha \frac{\partial f}{\partial x^\alpha} = \frac{m}{\tau}(f^{(0)} - f), \tag{15}$$

where $f^{(0)}$ is defined in Eq. (7) and $\tau$ is defined in Eq. (9). In the Marle model, there is no explicit definition of $\theta_E$ in [21]. Thus, we determine $\theta_E$ in the framework of Grad's 14 moments [19].

By multiplying both sides of Eq. (15) by $p^\beta p^\gamma$ and integrating in momentum space, we obtain

$$\partial_\alpha T^{\alpha\beta\gamma} = \frac{m}{\tau}(T_E^{\beta\gamma} - T^{\beta\gamma}), \tag{16}$$

where $T^{\alpha\beta\gamma} = \int_{\mathcal{R}^3} p^\alpha p^\beta p^\gamma f \frac{d^3\mathbf{p}}{p^0}$ and can be decomposed to yield [19]

$$T^{\alpha\beta\gamma} = (nC_1 + C_2\varpi)U^\alpha U^\beta U^\gamma + \frac{c^2}{6}(nm^2 - nC_1 - C_2\varpi)(\eta^{\alpha\beta}U^\gamma + \eta^{\alpha\gamma}U^\beta + \eta^{\beta\gamma}U^\alpha) + C_3(\eta^{\alpha\beta}q^\gamma + \eta^{\alpha\gamma}q^\beta + \eta^{\beta\gamma}q^\alpha) - \frac{6}{c^2}C_3(U^\alpha U^\beta q^\gamma + U^\alpha U^\gamma q^\beta + U^\beta U^\gamma q^\alpha) + C_4(p^{\langle\alpha\beta\rangle}U^\gamma + p^{\langle\alpha\gamma\rangle}U^\beta + p^{\langle\beta\gamma\rangle}U^\alpha). \tag{17}$$

Here, $p^{\langle\alpha\beta\rangle}$ is the pressure deviator, and $\varpi$ is the dynamic pressure. $C_1$, $C_2$, $C_3$ and $C_4$ in Eq. (17) are functions of $\zeta$ shown in [19].

Multiplying both sides of Eq. (16) by $U_\beta U_\gamma$ and eliminating terms with nonequilibrium projected moments ($p^{\langle\alpha\beta\rangle}$, $\varpi$, $q^\alpha$), we obtain

$$e_E - e = -\frac{\psi(\zeta_E)}{n}\nabla^\alpha U_\alpha, \tag{18}$$

where $\psi$ is defined in Eq. (C1). From Eq. (18), the energy density $e$ is not conserved by the collision term in the Marle model.

Multiplying both sides of Eq. (16) by $\Delta_{\beta\gamma}$ defined in Eq. (A6) with Eqs. (A12) and (17) and eliminating terms with nonequilibrium projected moments, we obtain

$$\varpi = -\eta(\zeta_E)\nabla^\alpha U_\alpha = -(\hat{\eta}(\zeta_E) + \tilde{\eta}(\zeta_E))\nabla^\alpha U_\alpha. \quad (19)$$

In Eq. (19), $-\hat{\eta}(\zeta_E)\nabla^\alpha u_\alpha$ is the dynamic pressure derived from either $p_E - p$ or $e_E - e$ on the right-hand side of Eq. (16) and $-\tilde{\eta}(\zeta_E)\nabla^\alpha U_\alpha$ is the dynamic pressure derived from the left-hand side of Eq. (16). If $\theta = \theta_E$, $-\hat{\eta}(\zeta_E)\nabla^\alpha u_\alpha = 0$ and $\varpi = -\tilde{\eta}(\zeta)\nabla^\alpha U_\alpha$. $\eta(\zeta)$ and $\tilde{\eta}(\zeta_E)$ are defined in Eqs. (C2) and (C3), respectively.

From Eqs. (18) and (19), $e_E$ is given by

$$e_E = e + \frac{\psi(\zeta_E)}{n\eta(\zeta_E)}\varpi. \quad (20)$$

From the approximate relation between $e$ and $p$ [19],

$$p_E - p = -\frac{n(e_E - e)}{1 - 5G_E\zeta_E - \zeta_E^2 + G_E^2\zeta_E^2} = \frac{nk(e_E - e)}{C_v(\zeta_E)}, \quad (21)$$

we obtain $\zeta_E$ or $\theta_E$ as

$$\frac{1}{\zeta_E} = \frac{1}{\zeta} + \frac{k\psi(\zeta_E)}{nmc^2C_v(\zeta_E)\eta(\zeta_E)}\varpi,$$
$$\theta_E = \theta + \frac{\psi(\theta_E)}{nC_v(\theta_E)\eta(\theta_E)}\varpi, \quad (22)$$

where $C_v$ is the constant-volume specific heat.

The Marle model, whose temperature of the gain term in its collision term is defined by Eq. (22), is called the modified Marle model.

## III. NUMERICAL METHOD OF SOLVING RELATIVISTIC BOLTZMANN EQUATION

The direct simulation Monte Carlo method [15] developed for nonrelativistic gases can be extended into relativistic gases. The Courant-Friedlichs-Lewy condition [22], which is required on the left-hand side of Eq. (1), requires that the time step $\Delta t$ approximates to zero when $p^\alpha \to \infty$, namely $v \to c$. Consequently, the left-hand side of Eq. (1) leads to the numerical stiffness via $\Delta t \to 0$ when we consider thermally relativistic flow. Thus, Eq. (5) is solved instead of Eq. (1).

As a numeric of the collision term in Eq. (5), the majorant frequency scheme [16] is used, whereas the past work [5,10] used the Bird's scheme [15], which calculates the collision-probability for all binary collision-pairs in the numerical cell. Consequently, the computational time required by the Bird's scheme is markedly longer than that by required by the majorant frequency scheme, because the majorant frequency scheme calculates the collision-pair the maximum collision number times. In the majorant frequency scheme, the maximum collision number during $\Delta t$ is obtained for a hard-sphere particle from Eq. (5) as

$$\nu_{\max} = \tfrac{1}{2}(N-1)n\gamma(u)\sigma_T(g_\varnothing)_{\max}\Delta t$$
$$= (N-1)nc\gamma(u)\sigma_T\Delta t(\because (g_\varnothing)_{\max} = 2c), \quad (23)$$

where $N$ is the number of sample particles in the cell. A collision pair is selected $\nu_{\max}$ times. The two particles selected induce a binary collision when the random number $\mathcal{W}$ $(0 < \mathcal{W} \le 1)$ satisfies

$$\frac{g_\varnothing}{(g_\varnothing)_{\max}} = \frac{g_\varnothing}{2c} < \mathcal{W}, \quad (24)$$

where $g_\varnothing$ is the Møller's relative velocity for the two particles selected.

Before and after the binary collision between particles 1 and 2, the total energy and total momentum of the binary particles must be conserved. The conservation of the energy $E$ and the momentum $\boldsymbol{p} = (p^1, p^2, p^3)$ before and after a binary collision is written as

$$E + E_* = E' + E'_* = E_{\rm tot}, \quad (25)$$

$$\boldsymbol{p} + \boldsymbol{p}_* = \boldsymbol{p}' + \boldsymbol{p}'_* = \boldsymbol{p}_{\rm tot}, \quad (26)$$

where $E = m\gamma(v)c^2$, $E_* = m\gamma(v_*)c^2$, $\boldsymbol{p} = m\gamma(v)\boldsymbol{v}$ and $\boldsymbol{p}_* = m\gamma(v_*)\boldsymbol{v}_*$. $E$ and $\boldsymbol{p}$ are related as follows:

$$E = \sqrt{c^2|\boldsymbol{p}|^2 + m^2c^4}. \quad (27)$$

In this paper, a binary collision is calculated using the following algorithm:

(a) Calculate the total energy ($E_{\rm tot}$) and total momentum ($\boldsymbol{p}_{\rm tot} = (p^1_{\rm tot}, p^2_{\rm tot}, p^3_{\rm tot})$) of binary particles from the left-hand sides of Eqs. (25) and (26).

(b) Redistribute the energy to binary particles, namely, $E'$ and $E'_*$, using a random number on the right-hand side of Eq. (26). From Eq. (27), the norms of momenta, namely, $|\boldsymbol{p}'|$ and $|\boldsymbol{p}'_*|$, are fixed.

(c) Decide the direction of the momentum by the law of cosines so that the total momentum is conserved in Eq. (26) as

$$\begin{pmatrix} p^{1'} \\ p^{2'} \\ p^{3'} \end{pmatrix} = \boldsymbol{M}(\phi, \varphi)\boldsymbol{N}(r)\begin{pmatrix} 0 \\ -|\boldsymbol{p}'|\sin\phi_1 \\ |\boldsymbol{p}'|\cos\phi_1 \end{pmatrix},$$
$$\begin{pmatrix} p^{1'}_* \\ p^{2'}_* \\ p^{3'}_* \end{pmatrix} = \boldsymbol{M}(\phi, \varphi)\boldsymbol{N}(r)\begin{pmatrix} 0 \\ -|\boldsymbol{p}'_*|\sin\phi_2 \\ |\boldsymbol{p}'_*|\cos\phi_2 \end{pmatrix}, \quad (28)$$

where $\phi_1$, $\phi_2$, $\boldsymbol{M}(\phi, \varphi)$ and $\boldsymbol{N}(r)$ are given by

$$\phi_1 = \arccos\left(\frac{|\boldsymbol{p}'|^2 + |\boldsymbol{p}_{\rm tot}|^2 - |\boldsymbol{p}'_*|^2}{2|\boldsymbol{p}'||\boldsymbol{p}_{\rm tot}|}\right),$$
$$\phi_2 = \arccos\left(\frac{|\boldsymbol{p}'_*|^2 + |\boldsymbol{p}_{\rm tot}|^2 - |\boldsymbol{p}'|^2}{2|\boldsymbol{p}'_*||\boldsymbol{p}_{\rm tot}|}\right) \quad (29)$$

$$\boldsymbol{M}(\phi,\varphi)=\begin{pmatrix}\cos\phi\cos\varphi & -\sin\varphi & \sin\phi\cos\varphi\\ \cos\phi\sin\varphi & \cos\varphi & \sin\phi\sin\varphi\\ -\sin\phi & 0 & \cos\phi\end{pmatrix},$$

$$\boldsymbol{N}(r)=\begin{pmatrix}\cos r & -\sin r & 0\\ \sin r & \cos r & 0\\ 0 & 0 & 1\end{pmatrix}, \tag{30}$$

where $r$ is a random number in the range of $0\le r\le 2\pi$, and $\phi$ and $\varphi$ are given by

$$\phi=\arccos\left(\frac{p^3_{\rm tot}}{|\boldsymbol{p}_{\rm tot}|}\right), \tag{31}$$

$$\begin{aligned}&\text{if } 0\le p^2_{\rm tot}\ \varphi=\arccos\left(\frac{p^1_{\rm tot}}{|\boldsymbol{p}_{\rm tot}|\sin\phi}\right)\\ &\text{else } 2\pi-\arccos\left(\frac{p^1_{\rm tot}}{|\boldsymbol{p}_{\rm tot}|\sin\phi}\right).\end{aligned} \tag{32}$$

## IV. NUMERICAL ANALYSIS OF RAREFIED SUPERSONIC FLOW OF THERMALLY RELATIVISTIC MATTER AROUND TRIANGLE PRISM

The rarefied supersonic flow of thermally relativistic matter around a triangle prism is numerically analyzed using the RBE, AW and MM models, and the forward regime of the triangle prism was solved focusing on the shock wave. Particles are assumed to be hard sphere particles with common mass $m$ and diameter $d$. For easier comprehension of the physical conditions, for the observer's frame, the absolute standard of rest is used as the hypothetical inertial frame. We use $(X, Y, Z)$ instead of $(x^1, x^2, x^3)$ and $(v^x, v^y, v^z)$ instead of $(v^1, v^2, v^3)$ and consider only the $XY$ plane, because a triangle prism has an infinite length in the $Z$ direction. Here, physical quantities in the uniform flow are written using the subscript $\infty$. As conditions of the uniform flow, $\zeta_\infty = 45$, and the velocity of the uniform flow is $u^x_\infty/c = 0.6$. The Mach number of the uniform flow, $M_\infty$, is 3.247 from the definition of the speed of sound in Eq. (10). The rarefaction parameter of the uniform flow, $\sigma_T n_\infty L$, which defines $1/(v_s\tau)$ in Eq. (4), is set to 10, where $L$ is the representative length in a flow field. For the numerical grids, $(v^x, v^y, v^z, X, Y) = (64, 64, 64, 64, 60)$ is used for the AW and MM models. For the calculation of the RBE using the DSMC method, 810 000 sample particles are used in the numerical grids $(X, Y) = (60, 80)$. Numerical tests indicate that the number of numerical grid for the AW and MM models and the number of sample particles for the RBE provide accurate simulations. Figure 1 shows the schematic of the flow field. We calculate the regime $0\le X$ and set the temperature $(\theta_w)$ of the wall to

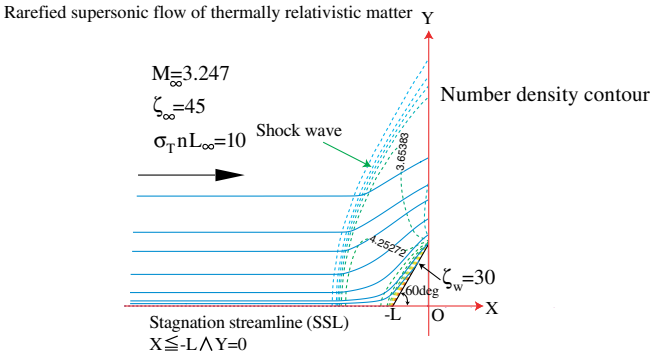


FIG. 1 (color online). Schematic of flow field.

$\zeta_w = mc^2/(k\theta_w) = 30$, as shown in Fig. 1. The model of complete diffusion on the wall is used.

Figure 2 shows the profiles of the density (top-left), velocity (top-right) and temperature (bottom-left) for the RBE, AW and MM models. The location of the shock wave obtained using the RBE is farther toward the wall than those obtained using the AW and MM models. The shock wave obtained using the RBE is thinner than those obtained using the AW and MM models, because we set $\langle g_\varnothing\rangle = v_s$ in Eq. (9) despite the true relation $1.38v_s(\zeta=0) < \langle g_\varnothing\rangle < 1.75v_s(\zeta=\infty)$ to compare the previous result obtained using the AW model [11] with the present result obtained using the RBE. Consequently, the lower collision frequencies for the AW and MM models than the collision frequency for the RBE yields thicker shock wave than that obtained using RBE. The thickness of the shock wave obtained using the AW model is thinner than that obtained using the MM model because of the higher collision rate at the high velocity for the AW model than for the MM model, as discussed in Ref. [14]. On the other hand, the boundary layer obtained using the RBE, which is the regime between the location of the peak temperature and the wall, is thicker than those obtained using the AW and MM models, whereas the thermal boundary layer obtained using the MM is similar in thickness to that obtained using the AW model. The thickness of the thermally boundary layer is related to the Prandtl number ($\Pr\equiv 5k/(2m)\mu/\lambda$) under a fixed $n_\infty\sigma_T L$. The smaller Pr yields the larger thermal boundary layer on SSL [23]. The bottom-right of Fig. 1 shows profiles of Pr along the SSL. As shown in the bottom-right of Fig. 1, the Pr obtained using the RBE is smaller than those obtained using the MM and AW models. The smallest Pr obtained using the RBE pushes the shock wave farther toward the wall than those obtained using the AW and MM models. The peak temperature behind the shock wave obtained using the AW model is higher than those obtained using the RBE and MM model, because the Pr obtained using the AW model is larger than those obtained using the RBE and MM model [24], as shown in the bottom-right of Fig. 1. On the other hand, the peak temperature behind the shock wave

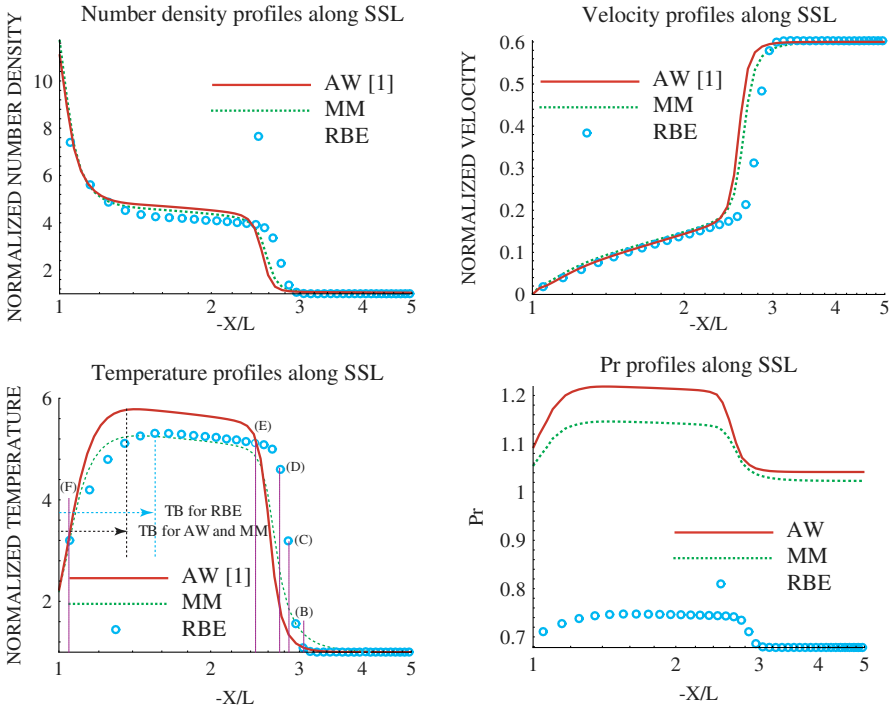


FIG. 2 (color online). Profiles of number density (top-left), velocity (top-right), temperature (bottom-left) and Prandtl number (bottom-right) along stagnation streamline. (TB: thermal boundary layer).

obtained using the RBE is larger than that obtained using the MM model despite the smaller Pr for the RBE than that for the MM model, because a thinner shock wave yields a higher peak temperature behind the shock wave in the rarefied regime [25].

Figure 3 shows the profiles of the heat fluxes $q^x$ and $q^x_{\rm NSF}$ defined in Eq. (A23) along the SSL for the RBE, AW and MM models on its left and the dynamic pressures $\varpi$ and $\varpi_{\rm NSF}$ defined in Eq. (A21) along the SSL for the RBE, AW and MM models. The heat fluxes $q^x$ obtained using the RBE, AW and MM models are not approximated by the RNSF law, namely, $q^x_{\rm NSF}$, inside the shock wave owing to the strong nonequilibrium state inside the shock wave. At $-X/L \le 1.15$, $q^x$ obtained using the RBE is smaller than $q^x$'s obtained using the AW and MM models, because the gradient of the temperature in the thermal boundary layer obtained using the RBE is smaller than those obtained using the AW and MM models, as shown in the bottom-left of Fig. 2. $q^x$ on the stagnation point, namely, $-X/L = 1.0$, is not obtained by the RBE, because physical quantities cannot be calculated on the surface of the cylinder using the DSMC method. The dynamic pressure $\varpi$ is not approximated by the RNSF law, namely, $\varpi_{\rm NSF}$ inside the shock wave and near the wall $1.0 \le -X/L < 1.2$. The signatures of $\varpi$ obtained using the RBE, AW and MM models are opposite to those of $\varpi_{\rm NSF}$ obtained using the RBE, AW and MM models. Additionally, magnitudes of $\varpi$ obtained using the RBE, AW and MM models are 10–$10^2$ times larger than those of $\varpi_{\rm NSF}$ obtained using the RBE, AW and MM models. Consequently, the dynamic

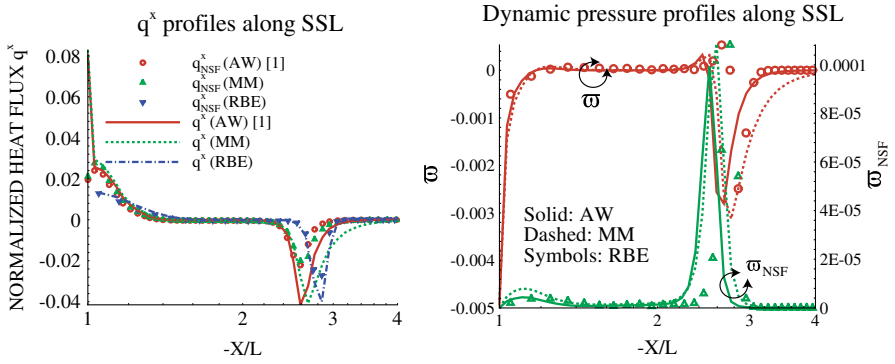


FIG. 3 (color online). Profiles of $q^x$ and $q^x_{\rm NSF}$ (left), and $\varpi$ and $\varpi_{\rm NSF}$ (right) along stagnation streamline.

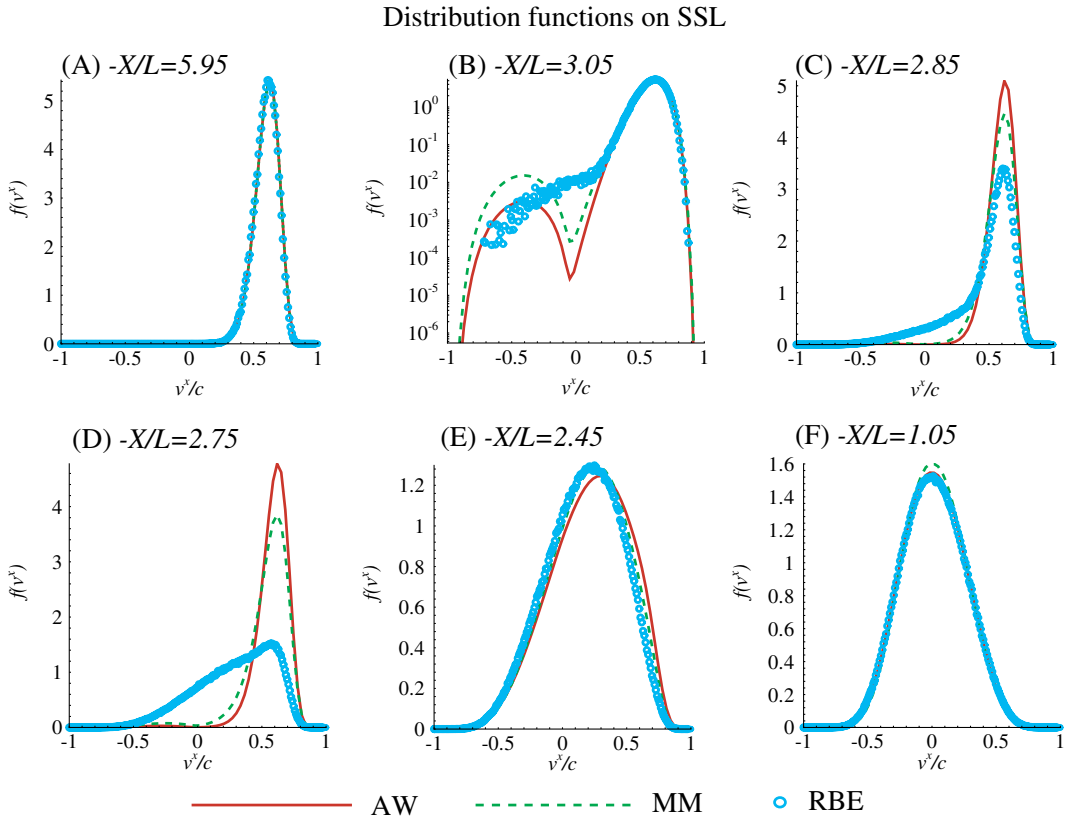


FIG. 4 (color online). Distribution functions on stagnation streamline at $-X/L = 5.95$ (A), 3.05 (B), 2.85 (C), 2.75 (D), 2.45 (E) and 1.05 (F).

pressure must be approximated by terms over the Burnett order [26] inside the shock wave and thermal boundary layer.

Finally, the distribution function $f(v^x) \equiv \frac{1}{n} \times \int_{\mathcal{V}^2} f\gamma(v)^5 dv^y dv^z$ on the SSL is considered. Figure 4 shows distribution functions at $-X/L = 5.95$ (A), 3.05 (B), 2.85 (C), 2.75 (D), 2.45 (E) and 1.05 (F) on the SSL. Points (B–F) are shown in the bottom-left of Fig. 2. At point (A), the distribution functions obtained using the RBE, AW and MM models are equal to the Maxwell-Jüttner function in the uniform flow. This reproduction of the Maxwell-Jüttner function in the uniform flow can be considered proof that our DSMC code for solving the RBE works correctly. At point (B), which corresponds to the rise of the shock wave as shown in the bottom-left of Fig. 2, $f_{\mathrm{RBE}}$, which is $f(v^x)$ obtained using the RBE, has a lower-negative-velocity tail at $-1.0 < v^x/c \leq -0.5$ than $f_{\mathrm{AW}}$, which is $f(v^x)$ obtained using the AW model, and $f_{\mathrm{MM}}$, which is $f(v^x)$ obtained using the MM model. Additionally, both $f_{\mathrm{AW}}$ and $f_{\mathrm{MM}}$ have bimodal forms, whereas $f_{\mathrm{RBE}}$ indicates not a bimodal form but a smooth deceleration of hard-sphere particles. These bimodal forms in $f_{\mathrm{AW}}$ and $f_{\mathrm{MM}}$ are caused by the Bhatnagar-Gross-Krook (BGK) [27]type collision term [28]. At points (C) and (D), $f_{\mathrm{RBE}}$ is quite different from $f_{\mathrm{AW}}$ and $f_{\mathrm{MM}}$, because the shock wave obtained using the RBE is thinner than those obtained using the AW and MM models. At point (E), where is the backward the shock wave for the RBE, $f_{\mathrm{RBE}}$ is similar to $f_{\mathrm{MM}}$, whereas $f_{\mathrm{AW}}$ is different from $f_{\mathrm{RBE}}$ and $f_{\mathrm{MM}}$. At point (F), which corresponds to the vicinity of the wall, $f_{\mathrm{RBE}}$ is similar to $f_{\mathrm{AW}}$, whereas $f_{\mathrm{MM}}$ is slightly different from $f_{\mathrm{RBE}}$ and $f_{\mathrm{MM}}$ at approximately $v^x/c = 0$.

## V. CONCLUDING REMARKS

The rarefied supersonic flow of thermally relativistic matter around a triangle prism was analyzed using the RBE as an initial study of the Mach cone generated by fast partons through the hot and dense matter during Au + Au collision in the RHIC. As a solver of the RBE, the conventional DSMC method for the nonrelativistic Boltzmann equation was extended to a new DSMC method for the RBE. The numerical results obtained using the RBE are compared with those obtained using the AW and MM models. The profiles of the number density, velocity and temperature along the SSL obtained using the RBE are different from those obtained using the AW and MM models in the shock wave and thermal boundary layer. In particular, the location of the shock wave obtained using the RBE is farther toward the wall than those obtained using the AW and MM models, because the thermal boundary layer obtained using the RBE is the thickest, which is

derived from the smallest Prandtl number obtained using the RBE. The shock wave obtained using the RBE is thinner than those obtained using the AW and MM models because of its larger collision frequency than those obtained using the AW and MM models. Heat fluxes along the SSL obtained using the RBE, AW and MM models can be approximated by the RNSF law except for the strong nonequilibrium regime inside the shock wave, whereas dynamic pressures obtained using the RBE, AW and MM models cannot be approximated by the RNSF law. The magnitudes of the dynamic pressures obtained using the RBE, AW and MM models are 10–$10^2$ times larger than those of dynamic pressures approximated by the RNSF law. As a result, the dynamic pressure must be approximated by terms above the Burnett order inside the shock wave and thermal boundary layer. Finally, distribution functions on the SSL obtained using the RBE are compared with those obtained using the AW and MM models. The distribution function inside the shock wave obtained using the RBE indicate not a bimodal form, which is obtained using the AW and MM models, but a smooth deceleration of thermally relativistic matter inside the shock wave.

## APPENDIX A: ECKART DECOMPOSITION AND RELATIVISTIC NAVIER-STOKES-FOURIER LAW

Multiplying both sides of Eq. (1) by $p^\alpha$ and $p^\alpha p^\beta$ and integrating in momentum space, we obtain conservation equations in terms of $N^\alpha = \int_{\mathcal{R}^3} c p^\alpha f \frac{d^3\mathbf{p}}{p^0}$ and $T^{\alpha\beta} = \int_{\mathcal{R}^3} c p^\alpha p^\beta f \frac{d^3\mathbf{p}}{p^0}$ as Mass conservation:

$$\partial_\alpha N^\alpha = 0. \tag{A1}$$

Momentum-energy conservation:

$$\partial_\alpha T^{\alpha\beta} = 0. \tag{A2}$$

According to Eckart [18], $N^\alpha$ and $T^{\alpha\beta}$ can be decomposed as follows:

$$N^\alpha = nU^\alpha, \tag{A3}$$

$$T^{\alpha\beta} = p^{\langle\alpha\beta\rangle} - (p + \varpi)\Delta^{\alpha\beta} + \frac{1}{c^2}(U^\alpha q^\beta + U^\beta q^\alpha) + \frac{en}{c^2}U^\alpha U^\beta, \tag{A4}$$

where $p^{\langle\alpha\beta\rangle}$ is the pressure deviator and $U^\alpha$ is the four velocity of flow defined by

$$U^\alpha = \gamma(u)(c, u^i), \tag{A5}$$

where $u^i$ is the $i$th component of the velocity of flow. $\Delta^{\alpha\beta}$ in Eq. (A4) is the projector defined by

$$\Delta^{\alpha\beta} = \eta^{\alpha\beta} - \frac{1}{c^2}U^\alpha U^\beta, \tag{A6}$$

where the Minkowski metric tensor $\eta^{\alpha\beta}$ or $\eta_{\alpha\beta}$ is given by

$$\eta^{\alpha\beta} = \eta_{\alpha\beta} = \mathrm{diag}(+1, -1, -1, -1). \tag{A7}$$

The projected moments ($n$, $p^{\langle\alpha\beta\rangle}$, $p$, $\varpi$, $q^\alpha$ and $e$) are obtained as [18]

$$n = \frac{1}{c^2}N^\alpha U_\alpha, \tag{A8}$$

$$p^{\langle\alpha\beta\rangle} = (\Delta^\alpha_\gamma\Delta^\beta_\delta - \tfrac{1}{3}\Delta^{\alpha\beta}\Delta_{\gamma\delta})T^{\delta\gamma} \tag{A9}$$

$$p + \varpi = -\frac{1}{3}\Delta_{\alpha\beta}T^{\alpha\beta}, \tag{A10}$$

$$q^\alpha = \Delta^\alpha_\gamma U_\beta T^{\beta\gamma}, \tag{A11}$$

$$e = \frac{1}{nc^2}U_\alpha T^{\alpha\beta}U_\beta. \tag{A12}$$

The Projected moments $n$, $u^i$, $p^{\langle\alpha\beta\rangle}$, $q^\alpha$ and $\varpi$ can be reduced from Eqs. (A8) and (A10) to 14 projected moments ($n$, $u^i$, $p^{ij}$, $q^i$, $\varpi$, [$i$, $j$ = 1, 2, 3)] as

$$p^{\langle\alpha\beta\rangle}U_\alpha = 0, \tag{A13}$$

$$q^\alpha U_\alpha = 0. \tag{A14}$$

Conservative equations in Eqs. (A1) and (A2) yield balance equations for $n$, $U^\alpha$ and $e$ [19] as follows:

$$Dn + n\nabla^\alpha U_\alpha = 0, \tag{A15}$$

$$\frac{nh_E}{c^2}DU^\alpha = \nabla^\alpha(p + \varpi) - \nabla_\beta p^{\langle\alpha\beta\rangle} + \frac{1}{c^2}\Big(p^{\langle\alpha\beta\rangle}DU_\beta - \varpi DU^\alpha - Dq^\alpha - q^\alpha\nabla_\beta U^\beta - q^\beta\nabla_\beta U^\alpha - \frac{1}{c^2}U^\alpha q^\beta DU_\beta - U^\alpha p^{\langle\beta\gamma\rangle}\nabla_\beta U_\gamma\Big), \tag{A16}$$

$$nDe = -(p + \varpi)\nabla_\alpha U^\alpha + p^{\langle\alpha\beta\rangle}\nabla_\beta U_\alpha - \nabla_\alpha q^\alpha + \frac{2}{c^2}q^\alpha DU_\alpha, \tag{A17}$$

where $D$, $\nabla^\alpha$ and the enthalpy per particle $h_E$ are defined by

$$D \equiv U^\alpha\partial_\alpha, \tag{A18}$$

$$\nabla^\alpha = \Big(\eta^{\alpha\beta} - \frac{1}{c^2}U^\alpha U^\beta\Big)\partial_\beta = \Delta^{\alpha\beta}\partial_\beta, \tag{A19}$$

$$h_E = e + \frac{p}{n}, \tag{A20}$$

where $\partial_\alpha \equiv \frac{\partial}{\partial x^\alpha}$. The Chapmann-Enskog expansion of the first order indicates that $\varpi$, $p^{\langle\alpha\beta\rangle}$ and $q^\alpha$ are approximated by the product of the temporal-spatial gradients of projected moments and transport coefficients, the bulk viscosity $\eta$, the viscosity coefficient $\mu$ and the thermal conductivity $\lambda$ as follows [19]:

$$\varpi = -\eta\nabla_\alpha U^\alpha, \tag{A21}$$

$$p^{\langle\alpha\beta\rangle} = 2\mu\left[\frac{1}{2}(\Delta^{\alpha}_{\gamma}\Delta^{\beta}_{\delta} + \Delta^{\alpha}_{\delta}\Delta^{\beta}_{\gamma}) - \frac{1}{3}\Delta^{\alpha\beta}\Delta_{\gamma\delta}\right]\nabla^{\gamma}U^{\delta} \tag{A22}$$

$$q^{\alpha} = \lambda\left(\nabla^{\alpha}\theta - \frac{\theta}{nh_E}\nabla^{\alpha}p\right) \tag{A23}$$

where $\eta$, $\mu$ and $\lambda$ for the RBE, AW and Marle models are given in Ref. [19]. In this paper, we used $\eta$, $\mu$ and $\lambda$ for the Marle model in place of those for the MM model under the assumption $\theta_E \simeq \theta$ in Eq. (22), when we calculate $q^{x}_{\mathrm{NSF}}$ and $\varpi_{\mathrm{NSF}}$ for the MM model in Sec. IV.

## APPENDIX B: NUMERICAL METHOD FOR SOLVING RELATIVISTIC BOLTZMANN-KINETIC MODELS

In general, the distribution function is $f = f(t, x^1, x^2, x^3, v^1, v^2, v^3)$, which has a one-to-one correspondence to $f = f(t, x^1, x^2, x^3, p^1, p^2, p^3)$. In this work, we use $f = f(t, x^1, x^2, x^3, v^1, v^2, v^3)$ instead of $f = f(t, x^1, x^2, x^3, p^1, p^2, p^3)$. To calculate the projected moments, we transform $d^3\mathbf{p}/p^0$ into the velocity space $d^3\mathbf{v}$ as

$$\frac{d^3\mathbf{p}}{p^0} = J\left|\frac{\partial p^i}{\partial v^j}\right|\Big/(m\gamma(v)c) = \frac{m^2\gamma(v)^4}{c}d^3\mathbf{v}. \tag{B1}$$

From Eq. (B1), the particle four-flow $N^{\alpha}$ can be written as

$$N^{\alpha} = c\int_{\mathcal{R}^3} p^{\alpha} f\frac{d^3\mathbf{p}}{p^0} = \int_{\mathcal{V}^3} m^3\gamma(v)^5(c, v^i)fd^3\mathbf{v}. \tag{B2}$$

The momentum-energy tensor $T^{\alpha\beta}$ can also be written as

$$T^{\alpha\beta} = c\int_{\mathcal{R}^3} p^{\alpha}p^{\beta}f\frac{d^3\mathbf{p}}{p^0} = \int_{\mathcal{V}^3} m^4\gamma(v)^6(c, v^i)(c, v^j)fd^3\mathbf{v}. \tag{B3}$$

In Eqs. (B2) and (B3), $\mathcal{V}^3$ is the velocity space stretched by $\{\mathcal{V}^3; |v| \le c\}$, where $|v| = \sqrt{(v^1)^2 + (v^2)^2 + (v^3)^2}$.

Projected moments, the number density $n$, the pressure deviator $p^{\langle\alpha\beta\rangle}$, the static pressure $p$, the dynamic pressure $\varpi$, the heat flux $q^{\alpha}$ and the energy per particle $e$ are obtained by Eckart decomposition using Eqs. (A8)–(A12). In a similar form to Eq. (5), the AW and MM models can be rewritten in the following form:

$$\frac{\partial f}{\partial t} + v^i\frac{\partial f}{\partial x^i} = \begin{cases}\left(\gamma(u)(c, u_i) + \frac{q^{\alpha}}{ne+p}\right)(c, -v^i)^T\frac{(f^{(0)}-f)}{c^2\tau} \text{ (AW model)}\\ \frac{1}{\gamma(v)\tau}(f^{(0)} - f) \text{ (MM model).}\end{cases} \tag{B4}$$

In our numerical code, the second order total variable diminishing scheme [22] is used for the left-hand side of Eq. (B4), and the second order Runge-Kutta time integration is used for the time integration of Eq. (B4).

For convenience, nondimensionalization is carried out using

$$\tilde{n} = \frac{n}{n_{\infty}}, \qquad \tilde{v}^i = \frac{v_i}{c}, \qquad \tilde{u}^i = \frac{u^i}{c}$$
$$\tilde{e} = \frac{e}{mc^2}, \qquad \tilde{q}^{\alpha} = \frac{q^{\alpha}}{n_{\infty}mc^3} \tag{B5}$$
$$\tilde{x}^i = \frac{x^i}{L}, \qquad \tilde{t} = \frac{t}{t_{\infty}}, \qquad t_{\infty} = \frac{L}{c},$$

where $L$ is the representative length in the observer's frame.

With these nondimensionalized quantities defined in Eq. (B5), the Maxwell-Jüttner function in Eq. (7) can be nondimensionalized as

$$\tilde{f}^{(0)} = \frac{(mc)^3}{n_{\infty}}f^{(0)} = \frac{\tilde{n}\zeta}{4\pi K_2(\zeta)}e^{-\zeta\gamma(\tilde{u})\gamma(\tilde{v})(1-\tilde{u}^i\tilde{v}^i)}. \tag{B6}$$

The left-hand side of Eq. (B4) represents the propagation of molecules with the velocity vector $(v^1, v^2, v^3)$ in the physical space $(x^1, x^2, x^3)$. This formulation for molecular propagation in such physical space does not involve relativistic effects. As a result, in the body-fitted curvilinear coordinates $(\xi^1, \xi^2, \xi^3)$, molecules with a velocity vector $(v^1, v^2, v^3)$ in $(x^1, x^2, x^3)$ propagate with a velocity $(v^1_{\xi}, v^2_{\xi}, v^3_{\xi})$. Equation (B4) can therefore be written in the body-fitted curvilinear coordinates $(\xi^1, \xi^2, \xi^3)$ as

$$\frac{\partial\hat{f}}{\partial t} + \frac{\partial v^i_{\xi}\hat{f}}{\partial\xi^i} = \begin{cases}\left(\gamma(u)(c, u_i) + \frac{q^{\alpha}}{ne+p}\right)(c, -v^i)^T\frac{(\hat{f}^{(0)}-\hat{f})}{c^2\tau} \text{ (AW model)}\\ \frac{1}{\gamma(v)\tau}(\hat{f}^{(0)} - \hat{f}) \text{ (MM model)}\end{cases} \qquad \hat{f} = f/J, \tag{B7}$$

where $J$ is the Jacobian between $x^i$ and $\xi^i$.

The wall condition must also be considered. In this paper, complete diffusion at the wall [19] is assumed. From the conservation of the mass flux to the wall and by setting the $\xi^2$ axis as the vector normal to the plane element of the wall, we obtain

$$f_w = f(v^2_{\xi} < 0), \tag{B8}$$
$$f_w/n_w = f^{(0)}(1, \theta_w, 0)(v^2_{\xi} \ge 0), \tag{B9}$$
$$n_w = \frac{-\int_{v^2_{\xi}<0} v^2_{\xi}f\gamma^5 d^3\mathbf{v}}{\int_{v^2_{\xi}\ge 0} v^2_{\xi}f_w/n_w\gamma^5 d^3\mathbf{v}}, \tag{B10}$$

where $f_w$ is the distribution function on the wall. $n_w$ is the number density reflected from the wall and $\theta_w$ is the temperature of the wall.

## APPENDIX C: DEFINITIONS OF $\psi(\zeta_E)$ IN EQ. (18), $\eta(\zeta_E)$ AND $\tilde{\eta}(\zeta_E)$ IN EQ. (19)

$\psi(\zeta_E)$ in Eq. (18) is given by

$$\psi(\zeta_E) = \tau mkc^2 \frac{20G_E + 3\zeta_E - 13G_E^2\zeta_E^2 - 2G_E^2\zeta_E^2 - 2G_E\zeta_E^2 + 2G_E^3\zeta_E^3}{\zeta_E C_v(\zeta_E)}, \tag{C1}$$

where $C_v(\zeta_E)$ is the constant-volume specific heat given by $C_v(\zeta_E) = k(\zeta_E^2 + 5G_E\zeta_E - G_E^2\zeta_E^2 - 1)$. The correct bulk viscosity for $\theta \neq \theta_E$ is given by [19]

$$\eta(\zeta_E) = \frac{\tau p_E k^2}{3} \frac{(20G_E + 3\zeta_E - 13G_E^2\zeta_E - 2G_E\zeta_E^2 + 2G_E^3\zeta_E^2)(4 - \zeta_E^2 - 5G_E\zeta_E + G_E^2\zeta_E^2)}{C_v(\zeta_E)^2}. \tag{C2}$$

The bulk viscosity for $\theta = \theta_E$ is given by

$$\tilde{\eta}(\zeta) = \frac{\tau pk^2}{3} \frac{(20G + 3\zeta - 13G^2\zeta - 2G\zeta^2 + 2G^3\zeta^2)(1 - \zeta^2 - 5G\zeta + G^2\zeta^2)}{C_v(\zeta)^2}. \tag{C3}$$


[1] K. Yagi, T. Hatsuda, and Y. Miyake, *Quark-Gluon-Plasma: From Big Bang to Little Bang* (Cambridge University Press, New York, 2005).
[2] http://www.bnl.gov/rhic/.
[3] http://www.lhc.ac.uk/.
[4] A. Dumitru, Y. Nara, B. Schenke, and M. Strickland, Phys. Rev. C **78**, 024909 (2008).
[5] Z. Xu and C. Greiner, Phys. Rev. C **71**, 064901 (2005).
[6] W. Israel, J. Math. Phys. (N.Y.) **4**, 1163 (1963).
[7] J. M. Stewart, *Non-equilibrium Relativistic Kinetic Theory*, Lecture Notes in Phys. Vol. 10 (Springer, Heidelberg, 1971).
[8] I. Müller and T. Ruggeri, *Rational Extended Thermodynamics* (Springer-Verlag, New York, 1998).
[9] F. Jüttner, Ann. Phys. (Berlin) **339**, 856 (1911).
[10] I. Bouras, E. Molnar, H. Niemi, Z. Xu, A. El, O. Fochler, C. Greiner, and D. H. Rischke, Phys. Rev. C **82**, 024910 (2010).
[11] R. Yano and K. Suzuki, Phys. Rev. D **83**, 023517 (2011); **83**, 049901(E) (2011).
[12] T. Renk and J. Ruppert, Phys. Rev. C **73**, 011901 (2006); B. Betz, J. Noronha, G. Torrieri, M. Gyulassy, I. Mishustin, and D. H. Rischke, Phys. Rev. C **79**, 034902 (2009); J. Casalderrey-Solana, E. V. Shuryak, and D. Teaney, J. Phys. Conf. Ser. **27**, 22 (2005).
[13] J. L. Anderson and H. R. Witting, Physica (Amsterdam) **74**, 466 (1974).
[14] R. Yano, K. Suzuki, and H. Kuroda, Physica A (Amsterdam) **381**, 8 (2007).
[15] G. A. Bird, *Molecular Gas Dynamics* (Clarendon Press, Oxford, 1976).
[16] M. S. Ivanov, S. V. Rogasinsky, and J. Russ, Russian Journal of numerical analysis and mathematical modelling **3**, 453 (1988).
[17] P. Danielewicz and G. F. Bertsch, Nucl. Phys. **A533**, 712 (1991).
[18] C. Eckart, Phys. Rev. **58**, 919 (1940).
[19] C. Cercignani and G. Kremer, *The Relativistic Boltzmann Equation: Theory and Applications, Progress in Mathematical Physics* (Springer-Verlag, Berlin, 2002), Vol. 22.
[20] L. D. Landau and E. M. Lifshitz, *Fluid Mechanics* (Pergamon Press, Oxford, 1987), 2nd ed..
[21] C. Marle, C.R. Acad. Sci. Paris **260**, 6539 (1965).
[22] H. C. Yee, *A Class of High-Resolution Explicit and Implicit Shock-Capturing Methods*, von Karman Institute for Fluid Dynamics, Lecture Series (NASA, Ames Research Center, Washington, D.C., 1989), Vol. 4.
[23] M. B. Abd-el-Malek and H. S. Hassan, Nonlinear Analysis: Modelling and Control **15**, No. 4, 379 (2010).
[24] The temperature behind the shock wave along the SSL increases as Pr increases. Such a tendency is confirmed in the nonrelativistic shock layer problem by solving the BGK model with Pr= 1 and the linear Fokker-Planck equation with Pr= 3/2. The temperature behind the shock wave along SSL obtained using the linear Fokker-Planck equation is higher than those obtained using the BGK model and nonrelativistic Boltzmann equation, which has Pr= 2/3, whereas the temperature obtained using the BGK model is higher than that obtained using the nonrelativistic Boltzmann equation as reported in Ref. [28].

[25] M. Ivanov, D. Khotyanovsky, A. Kudryavtsev, A. Shershneva, Y. Bondar, and S. Yonemura, in *Rarefaction and Non-equilibrium Effects in Hypersonic Flows about Leading Edges of Small Bluntness, Rarefied Gas Dynamics: 27th International Symposium on Rarefied Gas Dynamics*, edited by D. Levin, AIP Conf. Proc. No. 1333 (AIP, New York, 2011).

[26] L. L. Samojeden and G. M. Kremer, Physica A (Amsterdam) **307**, 354 (2002).

[27] P. L. Bhatnagar, E. P. Gross, and M. Krook, Phys. Rev. **94**, 511 (1954).

[28] R. Yano, K. Suzuki, and H. Kuroda, in *Consideration of the Vibrationally Linked Molecular Dissociation Model Based on the Kinetic Theory, Rarefied Gas Dynamics: 24th International Symposium on Rarefied Gas Dynamics*, edited by M. Capitelli, AIP Conf. Proc. No. 762 (AIP, New York, 2005).